Journal of Magnetism and Magnetic Materials 502 (2020) 166549

Contents lists available at ScienceDirect

Journal of Magnetism and Magnetic Materials

journal homepage: www.elsevier.com/locate/jmmm

Research articles

Structure and magnetic properties of $(Sm,Ho)_2Fe_{17}N_x$ (x = 0; 2.4)

S.V. Veselova[a], I.S. Tereshina[a,*], V.N. Verbetsky[a], D.S. Neznakhin[b], E.A. Tereshina-Chitrova[c,d], T.P. Kaminskaya[a], A.Yu. Karpenkov[a], O.V. Akimova[a], D.I. Gorbunov[e], A.G. Savchenko[f]

[a] Lomonosov Moscow State University, Leninskie Gory, 119991 Moscow, Russia
[b] Institute of Natural Sciences and Mathematics, Ural Federal University, 620002 Yekaterinburg, Russia
[c] Faculty of Mathematics and Physics, Charles University in Prague, Ke Karlovu 5, 12116 Prague, Czech Republic
[d] Institute of Physics, ASCR, 18221 Prague, Czech Republic
[e] Dresden High Magnetic Field Laboratory (HLD-EMFL), Helmholtz-Zentrum Dresden-Rossendorf, D-01314 Dresden, Germany
[f] National University of Science and Technology «MISIS», 4 Leninskiy prospekt, 119049 Moscow, Russia

ARTICLE INFO

Keywords:
Intermetallic compound
Microstructural analysis
Nitride
Ball milling
Crystal structure
Magnetic properties
Low temperatures
High magnetic fields

ABSTRACT

The structural and magnetic properties of the compound $Sm_{1.2}Ho_{0.8}Fe_{17}$ and the nitride powders $Sm_{1.2}Ho_{0.8}Fe_{17}N_{2.4}$ prepared by high energy ball milling under various milling regimes are reported. Magnetic properties of the samples are investigated at 2–300 K in steady magnetic field up to 70 kOe and in pulsed magnetic field up to 600 kOe. The application of high magnetic field reveals the presence of the second-order transition in $Sm_{1.2}Ho_{0.8}Fe_{17}N_{2.4}$ at 500 kOe. Magnetic hysteresis properties study shows that ball milling enhances magnetic performance of $Sm_{1.2}Ho_{0.8}Fe_{17}N_{2.4}$ making it perspective for the magnets fabrication.

1. Introduction

Advancement of modern technologies and invention of new devices demand involvement of new magnetic materials [1,2]. For instance, the application of hard magnetic materials is now relevant not only in the range of ambient and elevated temperatures but also at cryogenic temperatures. This is directly related to the widespread application of superconducting materials in the magnetic systems for various purposes [3,4].

As a rule, the use of the best permanent magnets of the Nd-Pr-Fe-B type is confined to 135 K. Below this temperature $(Nd_xPr_{1-x})_2Fe_{14}B$ ($0 < x \leq 1$) undergo a spin reorientation transition (except for $Pr_2Fe_{14}B$) [5–8] from easy-axis to cone magnetic anisotropy type. Another Fe-based permanent magnet (Fe ensures its low cost) with excellent properties $Sm_2Fe_{17}N_y$ [9] ($y \leq 3$) exhibits a strong uniaxial magnetic anisotropy (MA) in the whole temperature range of magnetic ordering and is promising for low-temperature applications. Deployment of advanced preparation techniques (such as gas-phase interstitial modification method) can help produce a high-coercivity state in the materials [10–14].

All rare-earth based magnets are multicomponent alloys with the hysteresis properties primarily determined by the composition and structure. Addition of heavy rare earths in $Nd_2Fe_{14}B$ enhances significantly coercivity and improves the magnets temperature stability [15–18]. Substitution both in the Fe [19–21] and R [22–26] sublattices affecting the structure and magnetic properties of $Sm_2Fe_{17}N_y$ have been extensively studied in recent decades. (Note that the Fe-sublattice behavior can be deduced from the studies of compounds with non-magnetic Rs, $Y(Lu)_2Fe_{17}$ [27–29]). While the impact of heavy rare-earths Tb, Dy and Er partially substituted for Sm was studied in great details [24,25], no information on the effects of Ho addition on magnetism of $Sm_2Fe_{17}N_y$ is available in literature.

In this paper, we study a combined influence of Ho substitution for Sm and nitrogen absorption on the magnetic hysteresis properties and high-field magnetization behavior of Sm_2Fe_{17}. The particular composition chosen for the study $Sm_{1.2}Ho_{0.8}Fe_{17}$ has an appreciably high saturation magnetization (knowing that the coupling between the Sm and Fe moments is parallel while it is antiparallel for Ho and Fe) and is apt for the study of competitive exchange interactions in high magnetic fields. The latter, if sufficiently strong, can break the antiparallel configuration of magnetic moments thus providing information on the inter-sublattice coupling strength in the *R*-Fe compounds. We further used interstitial modification by nitrogen, which is a powerful tool in changing the main magnetic characteristics (e.g. saturation

* Corresponding author.
E-mail address: tereshina@physics.msu.ru (I.S. Tereshina).

https://doi.org/10.1016/j.jmmm.2020.166549
Received 30 August 2019; Received in revised form 14 January 2020; Accepted 1 February 2020
Available online 03 February 2020
0304-8853/

magnetization, magnetic anisotropy type, etc.) of the *R*-Fe compounds [10]. The maximum nitrogen content we have been able to obtain in our $Sm_{1.2}Ho_{0.8}Fe_{17}N_y$ sample is $y = 2.4$. Further, fine powders $Sm_{1.2}Ho_{0.8}Fe_{17}N_{2.4}$ were prepared by high energy ball milling using various milling regimes to reveal their influence on the morphology, structure, phase composition and magnetic hysteresis properties of $Sm_{1.2}Ho_{0.8}Fe_{17}N_{2.4}$. The magnetic measurements were carried out at various representative temperatures, including low temperatures, with the use of high magnetic fields up to 600 kOe.

2. Experiment

The as-cast alloy $Sm_{2-x}Ho_xFe_{17}$ with $x = 0.8$ was prepared by induction melting of constituent elements of at least 99.9% purity, followed by annealing in vacuum at 1273 K for 8 days. Excess amount of Sm was added to a nominal composition of $Sm_{1.2}Ho_{0.8}Fe_{17}$ to prevent Sm evaporation losses during melting. The surface morphology and composition were studied by scanning electron microscopy (SEM) using a LEO EVO-50 XVP Zeiss electron microscope equipped with an EDX INCA-energy 350 analyzer with pure Sm, Ho, Fe as standards (Oxford Instruments).

Procedure of nitrogenation of the material was performed by heat treating the crushed into powder parent alloy in the pure nitrogen atmosphere with a pressure up to 40 atm at 450 °C for 24 h. We obtained a nitrogenated sample with 2.4 nitrogen atoms per formula unit (N at./f.u.). The error in the nitrogen content determination is 0.1 at.N/f.u.

The nitrided powders $Sm_{1.2}Ho_{0.8}Fe_{17}N_{2.4}$ (~5 g) were further subjected to the wet ball-milling in the stainless-steel bowl. The milling process was conducted at room temperature using a high-energy ball mill by Planetary Mono Mill PULVERISETTE 6 (Fritsch, Germany) with the diameter of the stainless-steel balls of 6.5 mm. Samples were milled for 15, 30, and 45 min at a rotating rate of 300 rpm. The ball-milled powders were dispersed and deagglomerated using ultra sound. The particles sizes of the milled powders were determined by a 20 kV-field emission SEM, supplied by TESCAN VEGA3 (Czech Republic) and the free software ImageJ.

The morphology of the powder after 45 min milling was investigated by an Atomic Force Microscopy (AFM) using a SMENA-A scanning probe microscope, the Solver platform (NT-MDT company, Russia). Scanning was performed with HA-NC ETALON silicon cantilevers with a resonance frequency of 140–225 kHz and a tip radius of 10–30 μm in contact and semi-contact modes. For measurements, the powdered sample was glued on a sticky tape forming a thin layer. AFM images were processed using the Nova 873 software for 2D and 3D AFM images.

The crystal structure of the as-cast and annealed alloys, and of the nitride samples before and after ball milling were characterized by x-ray diffraction (XRD) with CoKα radiation in a $2\theta = 20°$-$120°$ range on a DRON-4-07 diffractometer using a graphite monochromator. Magnetic measurements were performed on a powder samples fixed by wax using a SQUID magnetometer (Quantum Design, USA) in the temperature range 2–300 K and magnetic fields up to 70 kOe and a vibrating-sample magnetometer (VSM-250) at room temperature in magnetic field up to 20 kOe. The magnetization in pulsed magnetic fields up to 600 kOe was measured at the Dresden High Magnetic Field Laboratory. Absolute values of the pulsed-field magnetization were calibrated using the steady field data.

3. Results and discussion

3.1. Crystal structure studies

3.1.1. $Sm_{1.2}Ho_{0.8}Fe_{17}$

We first address the properties of the parent sample $Sm_{1.2}Ho_{0.8}Fe_{17}$. The microstructure analysis (Fig. 1(a)) showed that the as-cast ingot combines the main 2:17-type phase with some secondary phases which include α-Fe and Sm-rich phase in agreement with the reported binary Sm-Fe phase diagram [30]. Quantitative elemental analysis showed that the Sm-rich phase is (Sm,Ho)Fe_3. The areas at which the sample' composition was determined are shown in Fig. 1(a).

The SEM micrograph of the annealed $Sm_{1.2}Ho_{0.8}Fe_{17}$ alloy revealed that it is a two-phase sample consisting of the main 2:17-type phase (light gray contrast section in Fig. 1(b) and pure iron (black contrast section). According to the quantitative electron probe microanalysis the nominal composition of the main 2:17-type phase corresponds to $Sm_{1.2}Ho_{0.8}Fe_{17}$. The amount of the second phase, α-Fe was determined from the XRD as 8 wt%. Substitution of Sm for Ho does not change the structure of the Sm_2Fe_{17} compound. The sample crystallizes in the rhombohedral Th_2Zn_{17}-type of structure (space group $R\bar{3}m$, No.166).

The lattice constants *a*, *c*, the ratio *a/c* and the unit-cell volume *V* of Sm_2Fe_{17} (adopted from Refs. [10,25]) and $Sm_{1.2}Ho_{0.8}Fe_{17}$ are compared in Table 1. The substitution of Ho for Sm in Sm_2Fe_{17} results in the decreased unit cell volume of the 2:17 phase due to lanthanide contraction.

3.1.2. $Sm_{1.2}Ho_{0.8}Fe_{17}N_{2.4}$ before and after ball milling

The XRD study showed that $Sm_{1.2}Ho_{0.8}Fe_{17}N_{2.4}$ preserved the rhombohedral Th_2Zn_{17}-type structure after nitrogenation. The amount of the α-Fe phase and lattice parameters of $Sm_{1.2}Ho_{0.8}Fe_{17}N_{2.4}$ are given in Table 1. While we observed lattice expansion for the main phase of the nitrogenated compound (shift of diffraction peaks, not shown here), α-Fe phase absorbed nitrogen only very little. The lattice parameters of $(Sm,Ho)_2Fe_{17}N_y$ are provided by the combined influence of Ho substitution for Sm and nitrogen absorption. It can be seen from Table 1 that the unit cell volume of the nitride $Sm_{1.2}Ho_{0.8}Fe_{17}N_{2.4}$ has increased slightly as compared to that of $Sm_2Fe_{17}N_{2.3}$ [10] The volume expansion ΔV/V upon nitrogenation is about 6.5%.

We further studied the ball-milled $Sm_{1.2}Ho_{0.8}Fe_{17}N_{2.4}$ samples obtained at various milling conditions. The XRD study showed that with the increase of the milling time t_{mil} intensity and the shape (broadening) of Sm-Ho-Fe-N peaks change only very little. For milling times longer than 15 min, the intensities of the peaks of soft magnetic α-Fe phase do not grow. In general, the XRD patterns of all the samples look very similar. In contrast to the Sm-Fe-N powders under prolonged milling times [31], we practically do not observe amorphization of the Sm-Ho-Fe-N powders. As shown in Table 1, the lattice parameters do not vary much with respect to t_{mil}.

Fig. 2 compares the AFM images of the Sm-Ho-Fe-N powder before milling (a) (contact mode) and after high-energy ball milling for $t_{mil} = 45$ min (b) (semi-contact mode). As it is seen from Fig. 2 that particles of $Sm_{1.2}Ho_{0.8}Fe_{17}N_{2.4}$ powder before milling arrange themselves into a layered columnar structure, while particles form a dendritic structure in the sample after milling for 45 min. In other words the AFM study demonstrates that particles self-assemble differently before and after the milling.

Exact determination of the particle size using either AFM or SEM is difficult due to the particles agglomeration. The average particles size of the nitrided sample and of the milled powders determined using ultrasonic dispersion in combination with SEM is given in Table 2. We determine the particles size ranging as 0.5 (and less) to 25 μm prior to ball-milling. It is known [31,32] that with the increase of the milling time, coercivity H_c of the isotropic $Sm_2Fe_{17}N_y$ powders is considerably enhanced due to formation of single-domain particles. According to Refs. [33–36], the single-domain size of $Sm_2Fe_{17}N_3$ is about 0.3 μm. The particles sizes of our samples decrease with the milling time increase (see Table 2 and Fig. 3(a)–(c)).

Fig. 3 shows SEM micrographs of powder samples obtained at various milling conditions and their particles size distribution in the form of a histogram. The latter reveals the formation of large agglomerates.

We further noted another important property of the materials. The grinded nitride powders of $Sm_{1.2}Ho_{0.8}Fe_{17}N_{2.4}$ were found to be resistant to oxidation regardless of the milling time duration. The

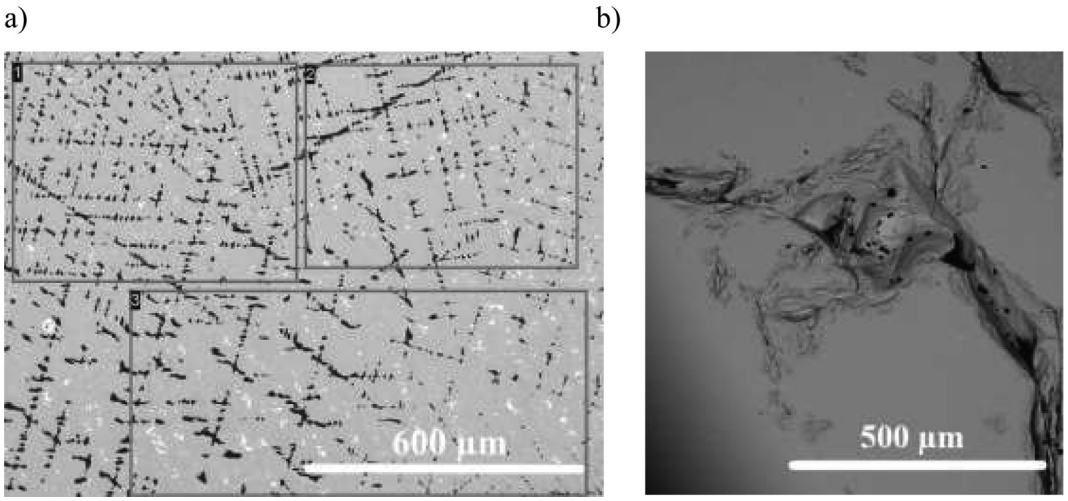

Fig. 1. SEM micrographs (BSE) of $Sm_{1.2}Ho_{0.8}Fe_{17}$: (a) as-cast sample and (b) the sample annealed at 1273 K. The $Sm_{1.2}Ho_{0.8}Fe_{17}$ phase is shown in grey, Sm-rich phase – in white, α-Fe – in black.

Table 1
Structural data of $(Sm_{1-x}Ho_x)_2Fe_{17}$, nitrided compounds and the ball-milled derivatives.

Composition	Milling time t_{mil}, min	α-Fe, wt.%	*a*, Å	*c*, Å	*c/a*	V, Å^3	ΔV/V, %
Sm_2Fe_{17} [10,25]	–	traces	8.55	12.43	1.454	786.9	–
$Sm_2Fe_{17}N_{2.3}$ [10,25]		–	8.73	12.64	1.448	833.7	6.3
$Sm_{1.2}Ho_{0.8}Fe_{17}$	–	8	8.522(0)	12.429(6)	1.458	782	–
$Sm_{1.2}Ho_{0.8}Fe_{17}N_{2.4}$	0	7	8.702(7)	12.698(9)	1.459	832.9	6.5
$Sm_{1.2}Ho_{0.8}Fe_{17}N_{2.4}$	15	7	8.696(7)	12.701(3)	1.461	831.9	–
$Sm_{1.2}Ho_{0.8}Fe_{17}N_{2.4}$	30	7	8.710(6)	12.711(0)	1.459	833.6	
$Sm_{1.2}Ho_{0.8}Fe_{17}N_{2.4}$	45	9	8.699(4)	12.710(5)	1.461	833.1	

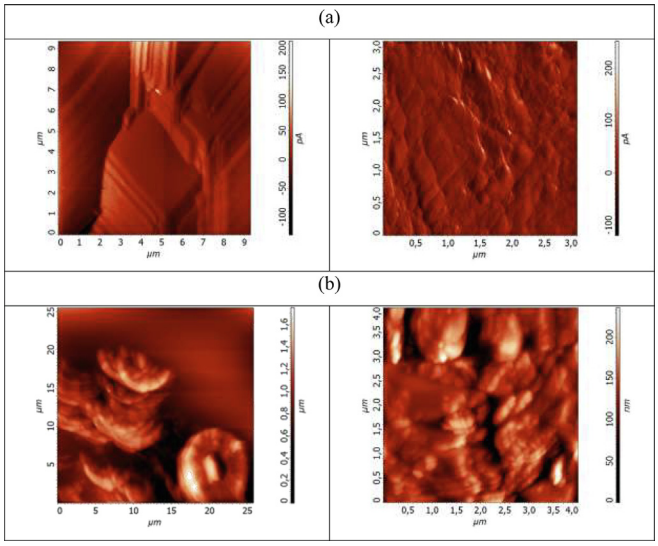

Fig. 2. AFM surface images of $Sm_{1.2}Ho_{0.8}Fe_{17}N_{2.4}$ powder before (a) and after (b) ball milling for 45 min at room temperature.

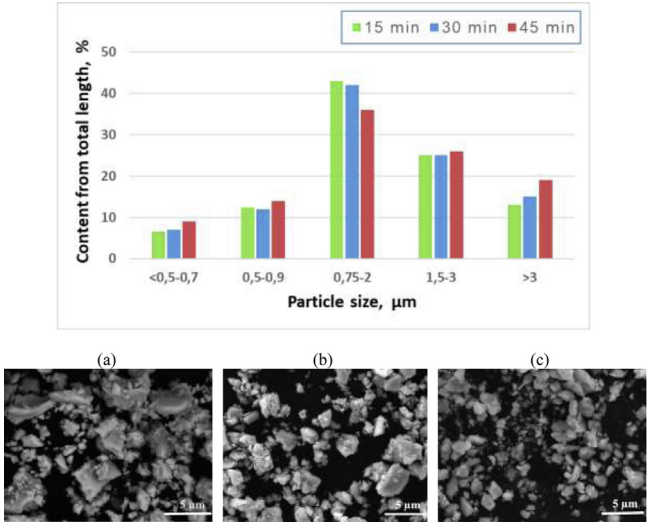

Fig. 3. Particle size distribution histogram (top) and SEM images of Sm-Ho-Fe-N ball-milled powders at RT (bottom) for 15, 30, 45 min and after ultrasonic dispersion (a, b, c), respectively.

Table 2
The magnetic characteristics of $Sm_{1.2}Ho_{0.8}Fe_{17}$ and its milled powders at $T = 300$ K.

Composition	Milling time, min	M_s, emu/g	H_c, kOe	$(BH)_{max}$, MG·Oe
$Sm_2Fe_{17}N_{2.3}$ [10,25]	0	140	–	–
$Sm_{1.2}Ho_{0.8}Fe_{17}N_{2.4}$	0	147	0.13	0
	15	120	2.68	3.0
	30	120	2.68	3.4
	45	109	3.46	3.1

conclusion is based on the XRD data (will be published elsewhere) which did not reveal any presence of oxide phases.

3.2. Magnetic properties study

3.2.1. $Sm_{1.2}Ho_{0.8}Fe_{17}$ and its nitride

The magnetic hysteresis loops of the parent $Sm_{1.2}Ho_{0.8}Fe_{17}$ and its nitride were previously measured in magnetic fields up to 20 kOe (not shown here). It was found that nitrogenation significantly changes the

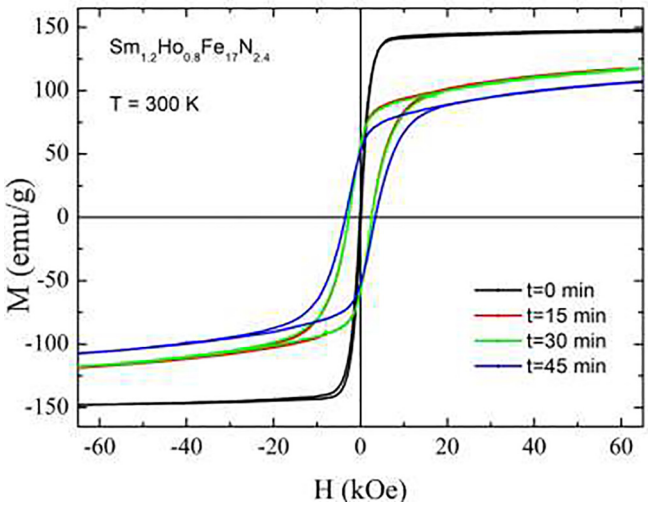

Fig. 4. Room-temperature hysteresis loops of $Sm_{1.2}Ho_{0.8}Fe_{17}N_{2.4}$ and its milled powders.

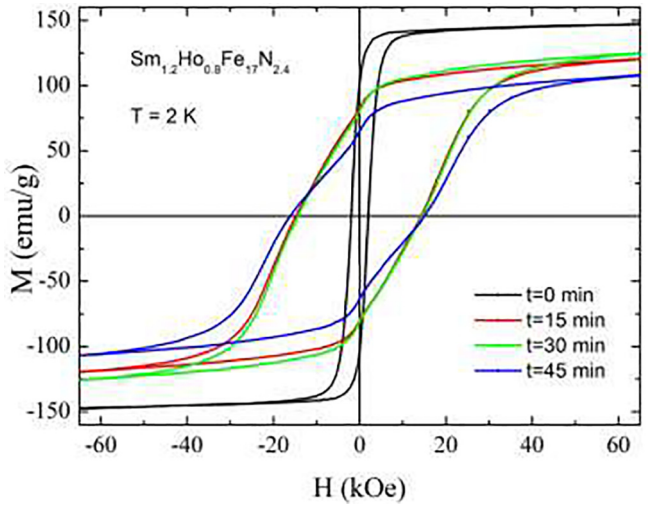

Fig. 5. Hysteresis loops of $Sm_{1.2}Ho_{0.8}Fe_{17}N_{2.4}$ and its milled powders at $T = 2$ K.

Table 3
The magnetic characteristics of $Sm_{1.2}Ho_{0.8}Fe_{17}$ and its milled powders at $T = 2$ K.

Composition	Milling time, min	M_s, emu/g	H_c, kOe	$(BH)_{max}$, MG·Oe
$Sm_{1.2}Ho_{0.8}Fe_{17}N_{2.4}$	0	149	1.96	9.4
	15	125	14.82	10.2
	30	123	14.29	9.5
	45	109	16.11	6.3

main magnetic characteristics of $Sm_{1.2}Ho_{0.8}Fe_{17}$, such as saturation magnetization, remanence and coercivity. Figs. 4 and 5 demonstrate hysteresis loops of $Sm_{1.2}Ho_{0.8}Fe_{17}N_{2.4}$ powders before and after ball-milling for different times measured at 300 and 2 K in magnetic field up to $H = 70$ kOe, respectively. Main magnetic characteristics at room temperature and at 2 K for $Sm_{1.2}Ho_{0.8}Fe_{17}$ and its nitride are collected in Tables 2 and 3, respectively. As seen from Table 2 saturation magnetization M_S of $Sm_{1.2}Ho_{0.8}Fe_{17}N_{2.4}$ is 147 emu/g. This value is slightly higher than that of the Ho-free $Sm_2Fe_{17}N_{2.3}$ at room temperature ($M_S = 140$ emu/g) [10,25]. The reason for this difference can be related both to the amount of nitrogen absorbed by the samples (2.4 and 2.3 at. N/f.u., respectively) and/or to the phase composition variation (Table 1).

We find that coercivity of the ball-milled Sm-Ho-Fe-N powders increases significantly as compared to the H_c of the nitrided material before milling. Indeed [33–36], the coercivity usually increases with the particle size decrease while the saturation magnetization decreases (see Tables 2 and 3). It can be seen from Table 2 that coercivities of powders milled for 15 and 30 min are nearly the same despite the particles size change (see Fig. 3). For $t_{mil} = 45$ min further increase of coercivity is observed with a simultaneous appearance of a kink in the second quadrant of the M − H curves. It was previously shown [31] that there are several reasons for the occurrence of such "kinks" in the crushed Sm-Fe-N powders. These may be associated with 1) the increasing amount of the soft magnetic phase (α-Fe) as a result of intensive and prolonged milling, 2) amorphization of Sm-Ho-Fe-N, and 3) agglomeration of powder particles during milling for more than 30 min. According to the XRD results two of the reasons can be immediately excluded: only a small increase in the amount of magnetically soft phase (1–2%) takes place in our case and the amount of amorphous phase in the $Sm_{1.2}Ho_{0.8}Fe_{17}N_{2.4}$ sample milled for 45 min is comparable with that before milling (Table 1). We may therefore link the observed kink to the high degree of particles agglomeration (see Fig. 2) during the prolonged high-energy milling for 45 min. Wendhausen et al. [36] showed that although agglomerates consist of single-domain crystallites, the size of the agglomerate is usually bigger that the single domain size.

The maximum magnetic energy product $(BH)_{max}$ of $Sm_{1.2}Ho_{0.8}Fe_{17}N_{2.4}$ and powder samples processed by milling calculated for $T = 300$ K and 2 K are listed in Tables 2 and 3, respectively. In our calculations, we used 7.0956 g/cm^3 as density calculated using XRD data and a demagnetizing factor of 1.6 (estimated for the used samples shape). The largest $(BH)_{max}$ values at 2 K are found for the $Sm_{1.2}Ho_{0.8}Fe_{17}N_{2.4}$ powders milled for 15 and 30 min, 10.15 MG·Oe and 9.51 MG·Oe, respectively. At the same time, the room temperature values of $(BH)_{max}$ are about three times lower and are independent of the milling time.

3.2.2. High magnetic field data

The magnetization curves $M(H)$ of $Sm_{1.2}Ho_{0.8}Fe_{17}N_{2.4}$ were measured in pulsed magnetic fields up to 600 kOe at temperatures 4–120 K (see Fig. 6). The smooth increase of magnetization from 149 to 165 emu/g ($\Delta M = 16$ emu/g) is observed when the magnetic field grows from 450 to 550 kOe. This growth is due to the presence of holmium moments in the sample. Indeed, in the R_2Fe_{17} compounds, the coupling between the rare earth and Fe moments is parallel for the first

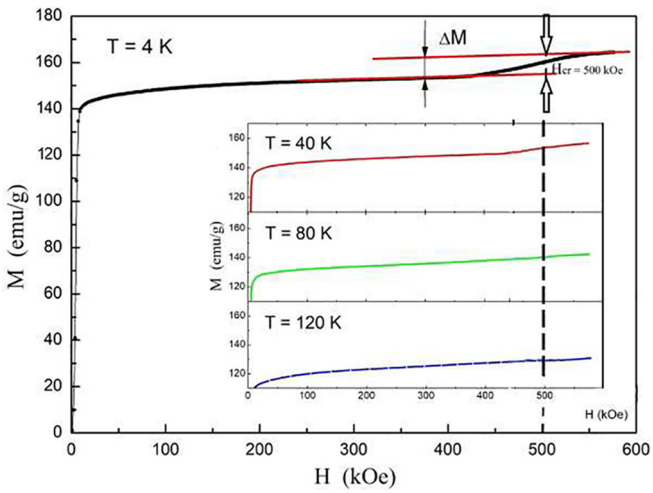

Fig. 6. Magnetization curves for $Sm_{1.2}Ho_{0.8}Fe_{17}N_{2.4}$ free powder measured in pulsed magnetic field at 4 K. The inset: the same at T = 40, 80 and 120 K.

half (Ce – Eu) and antiparallel for the second half (Gd – Yb) of the rare earth series. The antiparallel coupling between the rare earth and Fe moments can be broken by the magnetic fields of sufficient strength. The resulting curve will contain jumps (sudden increase of magnetization), by analyzing which the coupling strength between the sublattices can be estimated.

Skourski et al. [37] investigated the field dependence of magnetization $M(H)$ of a Ho_2Fe_{17} single crystal along different crystallographic directions in pulsed magnetic fields up to 600 kOe. They observed magnetization jumps at 450 and 550 kOe along the [1 2 0] and [1 0 0], respectively. The molecular field on the Ho sublattice was estimated as ~830–840 kOe. The spin-reorientation transitions in Ho_2Fe_{17} are clearly of the first order, with a small hysteresis [38]. The high-field magnetization increase in $Sm_{1.2}Ho_{0.8}Fe_{17}N_{2.4}$, on the contrary, is reminiscent of the second-order transition behavior (see Fig. 6). It should be noted that our magnetization measurements were carried out on free powder samples. However, similar $M(H)$ behavior was observed for the aligned (and fixed) powder of $Ho_2Fe_{17}N_2$ [39]. We may therefore assume that nitrogenation of $Sm_{1.2}Ho_{0.8}Fe_{17}$ is responsible for the transition type change from first to the second order.

The critical transition field (an inflection point on the high-field $M(H)$ curve) H_{cr} is ~ 500 kOe at T = 4 K in $Sm_{1.2}Ho_{0.8}Fe_{17}N_{2.4}$. This means that the partial substitution of Ho atoms for Sm in Ho_2Fe_{17} and further nitrogenation of the compound do not significantly change the critical transition fields. Indeed, we showed earlier [40,41] that the partial substitution of heavy rare earth (Ho) for light rare earth Nd (50%) in $Nd_1Ho_1Fe_{14}B$ does not change the exchange interactions between the Fe and Ho sublattices. The studies of the pseudoternary compounds $(Er,R)_2Fe_{14}B$ (R = Nd, Gd, Dy, Tm) [42,43] also demonstrated that these interactions do not change considerably when the composition varies. In $Sm_{1.2}Ho_{0.8}Fe_{17}N_{2.4}$, the strengthened magnetism of the Fe sublattice [44–47] resists the reduction of the inter-sublattice exchange due to the increased unit cell volume ($\Delta V/V$ = 6.5%) and as result, the transition field is ~500 kOe.

The dashed vertical line in the inset in Fig. 6 (used as a guide for the eye) allows us to observe transformation of the field-induced spin-reorientation transition with increasing temperature. ΔM is nearly zero at 120 K.

4. Conclusions

In this paper, we report on the structure and magnetic properties of the Sm-Ho-Fe-N powders prepared by high energy ball milling. $Sm_{1.2}Ho_{0.8}Fe_{17}N_{2.4}$ has a Th_2Zn_{17}-type of structure as the parent compound. Nitrogenation of the alloy boosts the unit-cell volume by more than 6%. Analysis of the particles size of milled powders shows that the increasing milling time promotes the appearance of agglomerates formed by the interacting particles. The agglomerates are of the micrometer size. The magnetic study shows that the ball-milling processing increases coercivity of materials. The largest $(BH)_{max}$ values at T = 2 K of 10.15 MG·Oe and 9.51 MG·Oe are found for the $Sm_{1.2}Ho_{0.8}Fe_{17}N_{2.4}$ powders milled for 15 and 30 min, respectively. The high-field study allowed us to observe a smooth growth of magnetization in $Sm_{1.2}Ho_{0.8}Fe_{17}N_{2.4}$ at fields ~500 kOe, while the single crystal of Ho_2Fe_{17} features two first-order transitions below and above this field (450 and 550 kOe). This finding allows us to conclude that exchange interactions between the magnetic sublattices leaves the critical field of the transition H_{cr} unchanged in $Sm_{1.2}Ho_{0.8}Fe_{17}N_{2.4}$. We observed a similar tendency for the $Ho_2Fe_{14}BH_x$ hydrides ($0 \le x \le 5.5$) [41]. The obtained fundamental and functional characteristics of $Sm_{1.2}Ho_{0.8}Fe_{17}N_{2.4}$ and observed regularities in the properties (structural and magnetic) formation upon various ball-milling processing times are essential for the development of hard magnetic materials for various applications at cryogenic and ambient temperatures.

Declaration of Competing Interest

The authors declare that they have no known competing financial interests or personal relationships that could have appeared to influence the work reported in this paper.

Acknowledgments

This work is performed with financial support of the grant of RSF (project № 18-13-00135). We acknowledge the support of HLD at HZDR, member of the European Magnetic Field Laboratory (EMFL). The work of E.A. T.-Ch. is supported by “Nanomaterials centre for advanced applications”, project no. CZ.02.1.01/0.0/0.0/15_003/0000485, financed by ERDF. The magnetic measurements in steady magnetic fields were performed in the Materials Growth and Measurement Laboratory (http://mgml.eu/) supported within the program of Czech Research Infrastructures (project no. LM2018096).

References

[1] J.M.D. Coey, Magnetism and Magnetic Materials, Cambridge University Press, 2010, p. 614, https://doi.org/10.1016/0304-8853(90)90756-G.
[2] K.H.J. Buschow, F.R. de Boer, Physics of Magnetism and Magnetic Materials, Kluwer Academic Publishers, New York, Boston, Dordrecht, London, Moscow, 2004, p. 191.
[3] P. Tixador, Y. Brunet, P. Brissonneau, M. Ivanes, Superconductors and rare earth magnets: an exciting combination for electrical motors, in: T. Sekiguchi, S. Shimamoto (Eds.), 11th International Conference on Magnet Technology, Springer, Dordrecht, 1990, pp. 621–626.
[4] T. Hara, T. Tanaka, H. Kitamura, T. Bizen, X. Maréchal, T. Seike, T. Kohda, Y. Matsuura, Cryogenic permanent magnet undulators, J. Phys. Rev. ST Accel. Beams 7 (2004) 050702, , https://doi.org/10.1103/PhysRevSTAB.7.050702.
[5] J.F. Herbst, $R_2Fe_{14}B$ materials: Intrinsic properties and technological aspects, Rev. Mod. Phys. 63 (1991) 819–898, https://doi.org/10.1103/RevModPhys. 63.819.
[6] A.S. Lileev, A.A. Parilov, M. Reissner, W. Steiner, Influence of the spin reorientation transition on the hysteresis characteristics of Nd-Fe-B film and bulk magnets, J. Magn. Magn. Mater. 270 (2004) 152–156, https://doi.org/10.1016/j.jmmm.2003.08.012.
[7] S.A. Nikitin, I.S. Tereshina, N.Yu. Pankratov, T. Palewski, H. Drulis, M.V. Makarova, Yu.G. Pastushenkov, Effect of hydrogenation on the magnetic characteristics of $Nd_2Fe_{14}B$ single crystal, Phys. Status Solidi (a) 196 (2003) 317–320, https://doi.org/10.1002/pssa.200306416.
[8] G.A. Politova, I.S. Tereshina, D.I. Gorbunov, M.A. Paukov, A.V. Andreev, R.M. Grechishkin, K. Rogacki, Magnetic and magnetocaloric properties of single crystal $(Nd_{0.5}Pr_{0.5})_2Fe_{14}B$, J. Alloys Compd. 751 (2018) 283–288, https://doi.org/10.1016/j.jallcom.2018.04.120.
[9] J.M.D. Coey, H. Sun, Improved magnetic properties by treatment of iron-based rare earth intermetallic compounds in ammonia, J. Magn. Magn. Mater. 87 (1990) L251–L254, https://doi.org/10.1016/0304-8853(90)90756-G.
[10] H. Fujii, H. Sun, Interstitially modified intermetallics of rare earth and 3d elements, Chapter 3, in: K.H.J. Buschow (Ed.), Handbook of Magnetic Materials, Elsevier Science B.V., 1995, , https://doi.org/10.1016/S1567-2719(05)80007-1.
[11] O. Gutfleisch, M.A. Willard, E. Bruck, C.H. Chen, S.G. Sankar, J.P. Liu, Magnetic materials and devices for the 21st century: Stronger, lighter, and more energy efficient, Adv. Mater. 23 (7) (2011) 821–842, https://doi.org/10.1002/adma.201002180.
[12] K.-H. Müller, L. Cao, N.M. Dempsey, P.A.P. Wendhausen, Sm_2Fe_{17} interstitial magnets, J. Appl. Phys. 79 (1996) 5045–5050, https://doi.org/10.1063/1.361568.
[13] H. Kronmüller, S. Parkin, Handbook of Magnetism and Advanced Magnetic Materials, Wiley, New York, 2007, p. 2912.
[14] J.M.D. Coey, Hard magnetic materials: a perspective, J. IEEE Trans. Magn. 47 (12) (2011) 4671–4681, https://doi.org/10.1109/TMAG.2011.2166975.
[15] W.F. Li, H. Sepehri-Amin, T. Ohkubo, N. Hase, K. Hono, Distribution of Dy in high-coercivity (Nd, Dy)–Fe–B sintered magnet, J. Acta Mater. 59 (2011) 3061–3069, https://doi.org/10.1016/j.actamat.2011.01.046.
[16] V.P. Menushenkov, A.G. Savchenko, Heat treatment, microstructure and coercivity of (Nd, Dy)-Fe-B based permanent magnets, J. Magn. Magn. Mater. 272–276 (2004) E1891–E1893, https://doi.org/10.1016/j.jmmm.2003.12.895.
[17] I.S. Tereshina, I.A. Pelevin, E.A. Tereshina, G.S. Burkhanov, K. Rogacki, M. Miller, N.V. Kudrevatykh, P.E. Markin, A.S. Volegov, R.M. Grechishkin, S.V. Dobatkin, L. Schultz, Magnetic hysteresis properties of nanocrystalline (Nd, Ho)-(Fe, Co)-B alloy after melt spinning, severe plastic deformation and subsequent heat treatment, J. Alloy. Compd. 68 (2016) 555–560, https://doi.org/10.1016/j.jallcom.2016.04.228.
[18] L. Hongjian, Y. Ming, L. Yuqing, W. Qiong, L. Weiqiang, Z. Dongtao, L. Qingmei, Crystal structure and magnetic properties of (Nd, $Tb_j2F_{e1}4B$ nanoflakes prepared by surfactant-assisted ball milling, J. AIP Adv. 7 (2017) 056231, , https://doi.org/10.1063/1.4978459.
[19] K.V.S. Rama Rao, H. Ehrenberg, G. Markandeyulu, U.V. Varadaraju, M. Venkatesan, K.G. Suresh, V.S. Murthy, P.C. Schmidt, H. Fuess, On the structural and magnetic

properties of R2Fe17-x(A, T)x (R – rare earth; A – Al, Si, Ga; T = transition metal) compounds, J. Phys. Stat. Sol. (a) 189 (2) (2002) 373–388.
[20] B.P. Hu, X.L. Rao, J.M. Xu, G.C. Liu, X.L. Dong, H. Li, L. Yin, Z.R. Zhao, Magnetic properties of $Sm_2(Fe_{1-x}M_x)_{17}N_y$ nitrides (M = Co, Ni, Al, Ti, V), J. Magn. Magn. Mater. 114 (1992) 138, https://doi.org/10.1002/1521-396X(200202)189:23.0.CO;2-G.
[21] M. Kubis, O. Gutfleisch, B. Gebel, K.-H. Muller, I.R. Harris, L. Schultz, Influence of M = Al, Ga and Si on microstructure and HDDR-processing of Sm(Fe, M) and magnetic properties of their nitrides and carbides, J. Alloys Comp. 283 (1999) 296–303, https://doi.org/10.1016/S0925-8388(98)00861-5.
[22] W.T. Pandey, M.-H. Du, D.S. Parker, Tuning the magnetic properties and structural stabilities of the 2–17-3 magnets $Sm_2Fe_{17}X_3$ (X = C, N) by substituting La or Ce for Sm, J. Phys. Rev. Appl. 9 (2018) 034002, , https://doi.org/10.1103/PhysRevApplied. 9.034002.
[23] M. Katter, J. Wecker, C. Kuhrt, L. Schultz, X.C. Kou, R. Grössinger, Structural and intrinsic magnetic properties of $(Sm_{1-x}Nd_x)_2Fe_{17}N_{=2,7}$ and $(Sm_{1-x}Nd_x)_2(Fe_{1-z}Co_z)_{17}N_{=2,7}$, J. Magn. Magn. Mater. 111 (1992) 293–300.
[24] M.Q. Huang, Y. Zheng, K. Miller, J.M. Elbicki, S.G. Sankar, Magnetism of (Sm, $R_)2F_{e1}7_Ny$ (R = Y, Tb or mischmetal), J. Appl. Phys. 70 (1990) 6024, https://doi.org/10.1063/1.350081.
[25] O. Tegus, Lu Yi, N. Tang, J.X. Wu, Yu Mingjun, Li Q.A. Li, R.W. Zhao, Yuan Jian, Y. Fuming, Magnetic properties of $(Sm_{1-x}R_x)_2Fe_{17}N_y$ (R = Dy Er) compounds, 2581–2583, J. IEEE Trans. Magn. 58 (1992), https://doi.org/10.1109/INTMAG.1992.696380.
[26] Y. Lu, O. Tegus, Q.A. Li, N. Tang, M.J. Yu, R.W. Zhao, J.P. Kuang, F.M. Yang, G.F. Zhou, X. Li, F.R. de Boer, Magnetic anisotropy of (Sm, $Y_)2F_{e1}7_Ny$ compounds, J. Phys. B 177 (1992) 243–246, https://doi.org/10.1016/0921-4526(92)90104-Z.
[27] S. Brennan, R. Skomski, O. Cugat, J.M.D. Coey, Anisotropy of easy-plane Y_2Fe_{17}, $Y_2Fe_{17}N_3$ and Sm_2Fe_{17}, J. Magn. Magn. Mater. 140–144 (1995) 971–972, https://doi.org/10.1016/0304-8853(94)01468-X.
[28] E.A. Tereshina, A.V. Andreev, J. Kamarad, H. Drulis, Magnetism of Lu_2Fe_{17}: The effects of Ru substitution, hydrogenation and external pressure, J. Alloys Comp. 492 (2010) 1–7, https://doi.org/10.1088/1742-6596/121/3/032010.
[29] E.A. Tereshina, A.V. Andreev, J. Kamarad, O. Isnard, Antiferromagnetic order in $(Lu_{0.8}Ce_{0.2})_2Fe_{17}$ and $Lu_2Fe_{16.}$ $5R_{u0.}5$: High pressure study, J. Appl. Phys. 105 (2009) 07A747, https://doi.org/10.1063/1.3075584.
[30] K.H.J. Buschow, The samarium–iron system, J. Less Common Metals 25 (1971) 131–134, https://doi.org/10.1016/0022-5088(71)90124-X.
[31] Q. Fang, X.F. An, Y. Wang, Li J. Du, W. Xia, A. Yan, J.P. Liu, J. Zhang, The structure and magnetic properties of Sm–Fe–N powders prepared by ball milling at low temperature, J. Magn. Magn. Mater. 410 (2016) 116–122, https://doi.org/10.1016/j.jmmm.2016.03.029.
[32] G. Hadjipanayis, D. Neil, A. Gabay, Ultrafine Sm-Fe-N Particles Prepared by Planetary Ball Milling, EPJ Web Conf. 40 (2013) 06006.
[33] G.J. Long, F. Grandjean, Supermagnets, Hard Magnetic Materials, Kluwer Academic Publishers, Netherlands, 1991.
[34] T. Mukai, T. Fujimoto, Kerr microscopy observation of nitrogenated Sm_2Fe_{17} intermetallic compounds, J. Magn. Magn. Mater. 103 (1992) 165–173, https://doi.org/10.1016/0304-8853(92)90250-R.
[35] J. Hu, T. Dragon, M.L. Sartorelli, H. Kronmüller, Investigation of the Domain Structure of $Sm_2Fe_{17}N_x$ Intermetallic Nitrides, J. Phys. Status Solidi. A 136 (1993) 207–214, https://doi.org/10.1002/pssa.2211360125.
[36] P.A.P. Wendhausen, B. Gebel, D. Eckert, K.H. Müller, Effect of milling on the magnetic and microstructural properties of $Sm_2Fe_{17}N_x$ permanent magnets, J. Appl. Phys. 75 (1994) 6018–6020, https://doi.org/10.1063/1.355494.
[37] Y. Skourski, M.D. Kuzmin, K.P. Skokov, A.V. Andreev, J. Wosnitza, High-field magnetization of Ho_2Fe_{17}, J. Phys. Rev. B 83 (2011), https://doi.org/10.1103/PhysRevB.83.214420.
[38] I.S. Tereshina, S.A. Nikitin, J. Stepient-Damm, W. Suski, A.A. Salamova, V.N. Verbetsky, Structure and magnetic properties of $Ho_2Fe_{17}H_X$ (x = 0; 3) single crystals, J. Magn. Magn. Mater. 258–259 (2003) 427–429, https://doi.org/10.1016/S0304-8853(02)01084-3.
[39] I.S. Tereshina, E.A. Tereshina-Chitrova, I.A. Pelevin, M. Doerr, J.M. Law, V.N. Verbetski, A.A. Salamova, High-Field Magnetization Study of $R_2Fe_{17}N_2$ (R = Ho and Er) Nitrides, J. Low Temp. Phys. 190 (2018) 236–243.
[40] N.V. Kostyuchenko, I.S. Tereshina, D.I. Gorbunov, E.A. Tereshina-Chitrova, A.V. Andreev, M. Doerr, G.A. Politova, A.K. Zvezdin, Features of magnetization behavior in the rare-earth intermetallic compound $(Nd_{0.5}Ho_{0.5})2Fe_{14}B$, J. Intermetallics 98 (2018) 139–142, https://doi.org/10.1016/j.intermet.2018.04.013.
[41] I.S. Tereshina, A.P. Pyatakov, E.A. Tereshina-Chitrova, D.I. Gorbunov, Yu. Skourski, J.M. Law, M.A. Paukov, L. Havela, M. Doerr, A.K. Zvezdin, A.V. Andreev, Probing the exchange coupling in the complex modified Ho-Fe-B compounds by high-field magnetization measurements, AIP Adv. 8 (2018) 125223, , https://doi.org/10.1063/1.5062588.
[42] M.R. Ibarra, Z. Arnold, P.A. Algarabel, L. Morellon, J. Kamarad, Effect of pressure on the magnetocrystalline anisotropy of $(Er_xR_{1-x})_2Fe_{14}B$ intermetallics, J. Phys. Condens. Matter. 4 (1992) 9721, https://doi.org/10.1088/0953-8984/4/48/024.
[43] I.S. Tereshina, L.A. Ivanov, E.A. Tereshina-Chitrova, D.I. Gorbunov, M.A. Paukov, L. Havela, H. Drulis, S.A. Granovsky, M. Doerr, V.S. Gaviko, A.V. Andreev, Tailoring the ferrimagnetic-to-ferromagnetic transition field by interstitial and substitutional atoms in the R-Fe compounds, Intermetallics 112 (2019) 106546, , https://doi.org/10.1016/j.intermet.2019.106546.
[44] T. Beuerle, M. Fahnle, Ab initio calculation of magnetic moments and hyperfine fields in $Y_2Fe_{17}Z_3$ (Z = H, C, N), Phys. Stat. Sol. (b) 174 (1992) 257–272.
[45] S.A. Nikitin, E.A. Ovtchenkov, I.S. Tereshina, V.N. Verbetsky, A.A. Salamova, Magnetocrystalline anisotropy and magnetostriction of H and N modified of R_2Fe_{17} compounds (R = Y, Tb, Dy, Ho, Er), J. Magn. Magn. Mater. 195 (1999) 464–469.
[46] E.A. Tereshina, H. Yoshida, A.V. Andreev, I.S. Tereshina, K. Koyama, T. Kanomata, Magnetism of a $Lu_2Fe_{17}H$ single crystal under pressure, J. Phys. Soc. Jpn. 76 (Suppl. A) (2007) 82–83.
[47] J.P. Liu, F.R. de Boer, P.F. de Châtel, R. Coehoorn, K.H.J. Buschow, On the 4f–3d exchange interaction in intermetallic compounds, J. Magn. Magn. Mater. 132 (1994) 159–179, https://doi.org/10.1016/0304-8853(94)90310-7.